ARTICLE IN PRESS

Available online at www.sciencedirect.com

SCIENCE DIRECT®

ELSEVIER

Experimental and Molecular Pathology xx (2005) xxx – xxx

Experimental and Molecular Pathology

www.elsevier.com/locate/yexmp

Multiplex PCR-based DNA array for simultaneous detection of three human herpesviruses, EVB, CMV and KSHV

Masahiro Fujimuro [a,*], Kazuhiro Nakaso [b], Kenji Nakashima [b], Hidetaka Sadanari [c], Inoue Hisanori [a], Yasuhiro Teishikata [a], S. Diane Hayward [d], Hideyoshi Yokosawa [a]

[a] *Department of Biochemistry, Graduate School of Pharmaceutical Sciences, Hokkaido University, Kita-ku, Sapporo 060-0812, Japan*
[b] *Department of Neurology, Institute of Neurological Sciences, Faculty of Medicine, Tottori University, 36-1, Nishicho, Yonago 683-8504, Japan*
[c] *Department of Microbiology and Immunology, Faculty of Pharmaceutical Sciences, Hokuriku University, Kanazawa, 920-1181, Japan*
[d] *Viral Oncology Program, Sidney Kimmel Cancer Center, Johns Hopkins School of Medicine, Baltimore, Maryland 21231, USA*

Received 15 September 2005

Abstract

Human lymphotropic herpesviruses, Epstein–Barr virus (EBV), cytomegalovirus (CMV) and Kaposi's sarcoma-associated herpesvirus (KSHV) are responsible for a wide variety of human diseases. Due to an increase in diseased states associated with immunosuppression, more instances of co-morbid infections with these herpesviruses have resulted in viral reactivations that have caused numerous fatalities. Therefore, the development of rapid and accurate method to detect these viruses in immunocompromised patients is vital for immediate treatment with antiviral prophylactic drugs. In this study, we developed a new multiplex PCR method coupled to DNA array hybridization, which can simultaneously detect all three human herpesviruses in one single cell sample. Multiplex PCR primers were designed to amplify specific regions of the EBV (EBER1), CMV (IE) and KSHV (LANA) viral genomes. Pre-clinical application of this method revealed that this approach is capable of detecting as few as 1 copy of the viral genomes for KSHV and CMV and 100 copies of the genome for EBV. Furthermore, this highly sensitive test showed no cross-reactivity among the three viruses and is capable of detecting both KSHV and EBV viral genomes simultaneously in the lymphoblastoid cells that have been double infected with both viruses. Thus, this array-based approach serves as a rapid and reliable diagnostic tool for clinical applications.

Keywords: Herpes virus; Epstein–Barr virus (EBV); Kaposi's sarcoma-associated herpesvirus (KSHV); Human herpesvirus 8 (HHV-8); Cytomegalovirus (CMV); Multiplex PCR; Diagnosis; DNA array

Introduction

Human lymphotropic herpesviruses, including Epstein–Barr virus (EBV), cytomegalovirus (CMV) and the more recently discovered Kaposi's sarcoma-associated herpesvirus (KSHV), are well known to be the etiological agents for pathogenesis in human (Jenner and Boshoff, 2002). Majority of the human population carries asymptotic infection of EBV and CMV. In the case of KSHV (also known human herpesvirus 8), the seropositivity rate in the normal adult population is only about 10–30%, which shows a specific tropism for people of Mediterranean and sub-Sahara African countries (Gao et al., 1996; Chatlynne et al., 1998). KSHV and EBV are oncogenic viruses with a long latency period in healthy hosts and will reactivate from dormancy when the hosts are immunosuppressed. Primary infections with these viruses in the immunocompetent host are generally asymptomatic. The neoplastic potentials of these two viruses have been well established, especially within the context of immunosuppressed patients who are undergoing bone marrow transplant or are co-infected with human immunodeficiency virus, HIV (Chang et al., 1994). The viral diseases of EBV and KSHV can range from lymphocytic leukemia to Burkitt's lymphoma, and from primary effusion lymphoma to erythromatous endothelial angiosarcoma, respectively. CMV does not have a true latency but certain cellular reservoirs harboring the virus are known to exist, and as a result, full virulent viremia can be triggered when immunosuppression takes place.

* Corresponding author. Fax: +81 11 706 4900.
E-mail address: fuji2@pharm.hokudai.ac.jp (M. Fujimuro).

0014-4800/$ - see front matter © 2005 Elsevier Inc. All rights reserved.
doi:10.1016/j.yexmp.2005.09.010

KSHV was initially identified in Kaposi's sarcoma, an endothelial neoplasm that is commonly associated with AIDS in homosexual men. It is also associated with primary effusion lymphoma and plasmablastic variant Multicentric Castleman's Disease (Ablashi et al., 2002). The latency-associated nuclear antigen (LANA) is encoded by ORF73 gene of the KSHV genome and is consistently expressed in KSHV-associated tumors. LANA is a multifunctional protein that ensures the association of viral genome with human genome via a tethering mechanism to facilitate viral DNA replication and effective segregation during cellular division (Ballestas et al., 1999). LANA also contributes to KSHV-associated oncogenesis through manipulation of cellular gene expressions. It interacts with tumor suppressor Rb (Radkov et al., 2000) and abolishes p53-mediated apoptosis (Friborg et al., 1999) as well as up-regulating the Wnt signaling pathway (Fujimuro and Hayward, 2004; Fujimuro et al., 2003).

EBV (human herpes virus 4) infects greater than 90% of the adult population worldwide (Hsu and Glaser, 2000). EBV is transmitted via saliva in an oral–fecal route of transmission, and it infects B lymphocytes as well as certain epithelial cells. EBV is linked to a number of human malignancies, including Burkitt's lymphoma, nasopharyngeal carcinoma and lymphoproliferative diseases in immunocompromised patients. EBV-encoded RNAs (EBERs) are the most abundant viral transcripts in latently EBV-infected cells, and its highly complex structural conformation enables it to bind to interferon-induced protein kinase R (Clarke et al., 1991; Nanbo et al., 2002).

CMV (human herpes virus 5) can be found in up to 90% of blood samples from immunocompromised patients (Espy et al., 1995). CMV remains a major threat for the medical management of immunosuppressed individuals since it is estimated that over one third of transplant recipients have acquired CMV viremia. CMV infection of the lung can cause severe therapy-resistant pneumonia or spontaneous pneumothoraces in AIDS patients, which are associated with a high mortality rate of over 50% (Goodrich et al., 1991). CMV is known to be present in saliva, cervical secretions, breast milk, semen and human lymphocytes (Numazaki and Chiba, 1997). During early phases of CMV infection, two immediate early (IE) genes, namely UL123 and UL122 (also known as IE1 and IE2, respectively), as well as other auxiliary viral genes, are expressed. CMV IE genes are thought to play critical roles in promoting the efficiency of CMV replication in host cells.

Polymerase chain reaction (PCR) technique has wide applications in a huge range of diagnostic uses involving various types of specimen analyses in a clinical setting. Multiplex PCR-based diagnostic assay can utilize different primers specific for different viruses in one single test, which means that it can combine different diagnostic tests for different viruses into one single comprehensive all-encompassing test. This approach is highly cost-effective and more efficient than ELISA types of serological analysis. However, even for multiplex PCR test, there remains a serious problem concerning data analysis which is limited by the long process of gel electrophoresis and requires further validation either by sequencing the PCR product or by hybridizing the PCR product to specific probes in a long and ancient Southern blot assay. With the advent of DNA array, this tedious and time-consuming process of data analysis involving Southern blotting or sequencing has been obviated. Hybridization of PCR products to a DNA array containing specific complementary DNA target probes allows instantaneous read-out of results, which greatly reduces time and the possibilities of human errors. Due to its unrestricted capacity to accommodate hundreds or even thousands of individual gene probes, a DNA array potentially allows for the simultaneous detection of all amplifiable DNA-based human pathogens present in a single specimen. As a result, this technology is ideal for parallel identification and differentiation of various viral pathogens in one sample, and this technique has already become a practical tool for the identifications of bacteria (Chizhikov et al., 2001) as well as for the genotyping of influenza viruses and HIV subtypes (Li et al., 2001; Wilson et al., 2000).

A few reports for DNA array-based detection of human lymphotropic herpesviruses have been described (Foldes-Papp et al., 2004; Striebel et al., 2004; Boriskin et al., 2004; Wang et al., 2002), and unfortunately, the DNA array approach has not yet been extended to the clinical diagnosis of lymphotropic herpesvirus infections because of high threshold of detection and low sensitivity toward samples with low virus copy numbers or due to a lack of standardized analysis protocol that allows for comparison between studies.

In this pre-clinical study, we describe the standardized protocol of a hybrid test combining multiplex PCR with DNA array technology to simultaneously detect EBV, CMV and KSHV genomes as well as external/internal control genes from single specimen. We examined the sensitivity and specificity of this test on established B cell lines isolated from a patient suffering from KSHV infection (BC3 cells), from a patient suffering from EBV-positive Burkitt's lymphoma (Raji cells), from a patient suffering both KSHV and EBV infections (BC2 cells) and from a patient with no known EBV/KSHV infections (DG75 cells). Since no cell lines are known to stably harbor CMV, a primary infection model was adopted by exposing susceptible human embryonic lung fibroblasts cells (HEL) to primary CMV infection in vitro to mimic CMV-infected cells in therapy-resistant pneumonia or spontaneous pneumothoraces. It was found that these cell samples closely resemble typical patient samples derived from centrifuged blood samples in a clinical setting and are perfect models for the pre-clinical phase of development for this new diagnostic technique.

Materials and methods

Cell line and extraction of viral DNA

KSHV-positive B lymphoblastoid cells (BC2 and BC3) were isolated from patients suffering from KSHV-mediated primary effusion lymphoma (PEL); EBV-positive B lymphoblastoid cells (Raji) were isolated from a patient suffering from Burkitt's lymphoma; and herpesvirus-negative B lymphoblastoid cells (DG75) were isolated from another patient suffering from Burkitt's lymphoma. All transformed B cells were grown in 10% FBS RPMI medium 1640 (Fujimuro and Hayward, 2003). To prepare viral genomic DNA, 1×10^5 of PEL or Raji cells were harvested, and the total DNAs from these cells were purified with a commercial DNA extraction kit (GenElute Mammalian Genomic midiprep kit, Sigma) to extract genomic DNA as well as viral DNA. Human embryonic lung

fibroblast cells (HEL) were grown in 10% FBS DMEM and were seeded at 1 × 10^6 per a 10 cm plate for a subsequent infection by CMV (Towne strain) at a MOI of 1. HEL cells were harvested, and viral DNA was extracted with the GenElute kit seven days post-CMV infection.

Cloning of PCR-amplified viral DNA

To accurately determine viral geonome copy number for the use of PCR template in the sensitivity evaluation phase of this study, fragments of KSHV LANA, EBV EBER1 and CMV IE genes were amplified with specific primers (shown in Table 1) and cloned into the pGEM-T plasmids (Promega), and the sensitivity of the DNA array (i.e., threshold of detection) was tested at different known numbers of viral gene-containing plasmid templates (one plasmid is considered to be equivalent to a single viral genome). Recombinant plasmids were propagated in DH5-α bacteria and purified with Wizard Plus SV Minipreps DNA Purification System (Promega).

Primers

The specific viral genes targeted by the multiplex PCR, sets of seven multiplex PCR oligonucleotide primers and the sequences of DNA probes immobilized on the DNA array membrane are listed in Table 1. All primer sequences were designed by Primer 3 (Whitehead Institute, and elaborated by Steve Rozen and Helen J. Skaletsky in 1996 and 1997). KSHV LANA, EBV EBER1 and CMV IE were selected as the target genes for PCR amplification and detection, and the PCR products yielded 346-bp, 167-bp and 347-bp fragments for LANA, EBER1 and IE, respectively. These sequences are accessible with the following GenBank accession numbers: AF360120, V01555 and AY315197 for LANA, EBER1 and IE genes, respectively. Internal controls, aminolevulinate delta-synthase 1 (ALAS1) gene and glyceraldehyde-3-phosphate dehydrogenase (GAPDH) gene, were also used for the multiplex PCR approach, and their sequences are accessible with the GenBank accession numbers NM 000688 and NM 002046, respectively.

Preparation of DNA array

DNA array probes for detecting viral DNA fragments as well as internal/external control gene fragments were spotted and immobilized on a nylon DNA array membrane. Spotting patterns consisted of seven parallel lines with five spots in each line, and each individual line of five spots is specific for a single gene, and the average signals from all five spots within the single line were used for the determination of detection sensitivity. To prepare the DNA array probes, viral DNA and internal/external control DNA fragments were amplified by PCR (denaturation for 5 min at 95°C; 30 cycles at 95°C for 30 s, 55°C for 30 s and 72°C for 30 s; and extension at 72°C for 5 min) with the viral gene-containing plasmid DNA as PCR templates. PCR products were then purified with the QIAQUICK 8 PCR Purification kit (QIAGEN) and resuspended in 100 μl of distilled water containing 10% (v/v) xylencyanol. The mixtures were spotted by hand on nylon membrane Hybond-N+ (Amersham Biosciences) with 0.2 μl (4 ng) of DNA for each spot. The DNA was subsequently cross-linked to the membrane with GS Gene Linker UV Chamber (BIORAD).

Table 1
Genes targeted for multiplex PCR and hybridization

Virus	Target gene[a]	Name[b]	Primer sequence	Product (bp)
KSHV	LANA	KSLA2/F	TTGGGAAAGGATGGAAGACG	346
		KSLA2/R	AGTCCCCAGGACCTTGGTTT	
EBV	EBER1	Eer1/F	AAAACATGCGGACCACCAGC	167
		Eer1/R	AGGACCTACGCTGCCCTAGA	
CMV	IE	CIE01/F	ATGTACGGGGGCATCTCTCT	347
		CIE01/R	GGGATAGTCGCGGGTACAG	
Internal control				
I1	ALAS1	ALAS1/F	CCAGACTCAACTCCCTCGAC	248
		ALAS1/R	GGCAGGGAAGACTCTTAGGG	
I2	GAPDH	GAPDH/F	GATCATCAGCAATGCCTCCT	496
		GAPDH/R	GCTTGACAAAGTGGTCGTTG	
External control[c]				
E1	Unknown	Pd-a/F	GTAGGAATCCTCGCGCAAT	242
		Pd-a/R	CCCACGCTAAGACAGGTGAA	
E2	Unknown	Pd-b/F	GAAGCGACGTTCAGTTGGAT	251
		Pd-b/R	ACCTGATCCGTGCAGACCTA	

[a] The genetic locus targeted by the described PCR primers. LANA, latent nuclear antigen; EBER, EBV-encoded RNA; IE, immediate-early gene; ALAS1, aminolevulinate synthase; GAPDH, glyceraldehyde-3-phosphate dehydrogenase.

[b] F, forward primer; R, reverse primer.

[c] External control (E1, E2) genes were cloned from *Burevundimonas diminuta*.

Amplification and labeling of target genes by multiplex PCR

For detection of virus in B lymphoblastoid and HEL cells, the genomic DNA extracts from various virus-infected cells (or 5 copies of control plasmid in the control experiment) were mixed with the PCR reaction solution. The reaction mixture (total of 25 μl) consisted of 1× PCR buffer, 1 unit of Ex Taq (Takara Bio Inc.), 2 mM dNTP, 2 mM biotinylated dUTP, 1 pmol of each specific primer pairs for KSHV LANA, EBV EBER1, HCMV IE or internal/external control (see Table 1) and 1 μl of sample genomic DNA as template. PCR reaction was carried out as follows: denaturation for 5 min at 95°C; 30 cycles at 95°C for 30 s, 55°C for 30 s and 72°C for 30 s; and extension at 72°C for 5 min. PCR products were precipitated with ethanol, air dried and resuspended in distilled H_2O for subsequent loading onto DNA array.

Hybridization and detection of signals

The DNA samples were denatured at 100°C for 5 min and loaded onto the probe-mounted DNA array membranes for hybridization at 68°C for 10 h. After hybridization, the membranes were washed three times with 2 × SSC and 0.1% SDS solutions at 68°C for 5 min each and subsequently three times with 0.1 × SSC and 0.1% SDS solutions at 68°C for 5 min each. The membranes were then processed with the Phototope-Star detection kit for nucleic acids (New England Biolabs) according to the manufacturer's recommendations. The chemiluminescent imaging analysis was carried out, and the images were documented by Fluor-S MAX2 Multi Imaging System (BIORAD).

External/internal positive controls for multiplex PCR and DNA array

Since low sensitivity is an inherent problem in virus detection system due to varying DNA quality or human handling errors, external and internal positive controls were included in our experiments. ALAS1 and GAPDH genes were amplified as human genomic internal controls, and DNA fragments derived from *Brevundimonas diminuta* were used as external controls. PCR products were also checked by gel electrophoresis to ensure proper fragment length prior to loading on the DNA array.

Results and discussion

Specificity of PCR-based DNA array hybridization in detecting different human herpesviruses

In this study, we developed the simultaneous detection method for all three pathogenic herpesviruses, namely EBV, CMV and KSHV, from a single cell sample specimen. Fig. 1 shows the schematics of the basic experiment design of our multiplex PCR detection method coupled to DNA array. This method consists of multiplex PCR amplification to simultaneously detect EBV, CMV and KSHV genomes that are expected to be present in a single cell sample, and DNA hybridization-based DNA array allows for accurate reading of the PCR

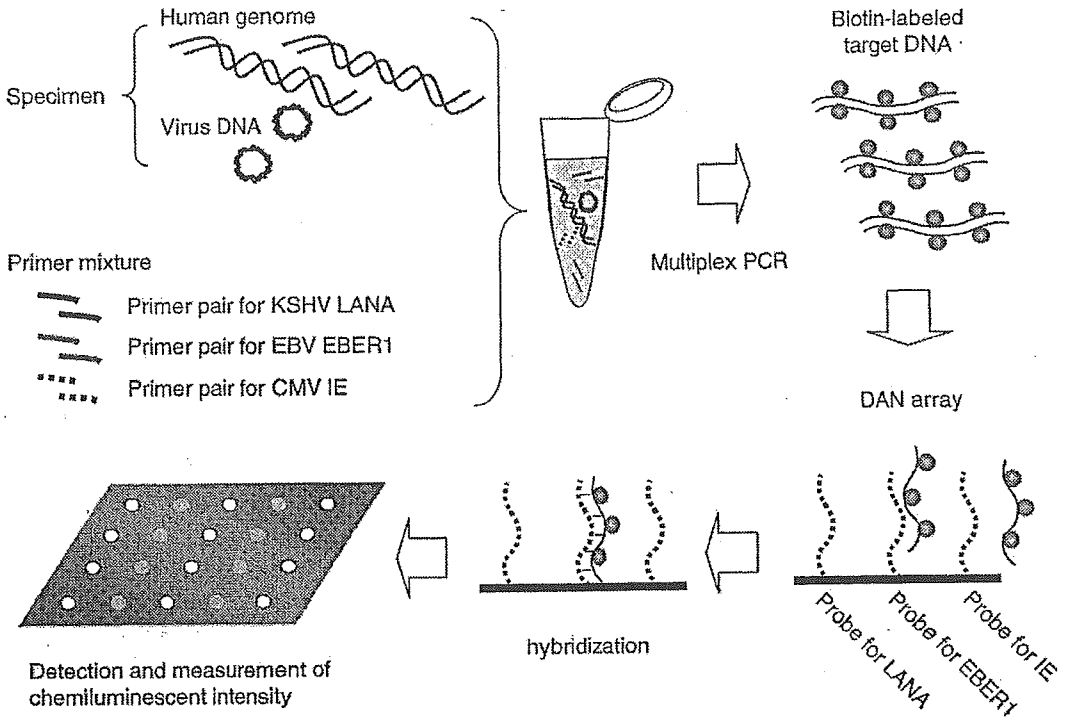

Fig. 1. Schematic diagram showing the procedures for the multiplex PCR-based DNA array hybridization method for simultaneous detection of EBV, CMV and KSHV. Portions of the EBV EBER1, the CMV IE and the KSHV LANA genes were amplified and biotin labeled by multiplex PCR amplification with virus-specific primers from a genomic DNA extract of target cells. Amplified target DNA fragments conjugated with biotin were hybridized to DNA probes for EBER1, IE and LANA genes immobilized on the DNA array and were then subjected to washing and subsequent detection of chemiluminescent signals.

products to ensure high sensitivity and specificity of the result. The multiplex PCR primers (their sequences are shown in Table 1) were designed to specifically and simultaneously amplify different viral genes present in a single cell sample, namely the EBER1 gene for EBV, IE gene for CMV and LANA gene for KSHV. However, due to the varying GC contents of the target template DNA sequence as well as the varying quality and concentrations of the polymerase enzymes, PCR technique occasionally produces non-specific products that yield the same length fragment as the correct product, or it produces low concentration of amplified products which falls below the threshold of detection by gel electrophoresis. Furthermore, human handling error accounts for a large percentage of errors in PCR-based diagnostic approaches.

To increase the specificity and sensitivity of amplified signals in multiplex PCR-based diagnostic approach, we coupled the DNA array hybridization method, which is great for validation of the amplified viral DNA fragments, to our multiplex PCR method. DNA array nylon membranes contained pre-mounted DNA probes for KSHV, EBV and CMV gene fragments as well as for internal and external control DNA fragments. These oligonucleotide DNA probes were PCR amplified from viral gene-containing DNA plasmids using specific primers (Table 1). After separating the PCR products from the PCR reaction mixtures, the amplified products were spotted as seven parallel lines consisting of 5 identical spots each and then immobilized onto the nylon membrane via UV cross-linking. Each line of 5 identical spots represents a single virus detection lane, and the varying signal intensities from the 5 spots are averaged to yield the mean signal intensity for sensitivity reading (Fig. 2A).

Total genomic DNA harvested from herpesvirus-infected primary effusion lymphoma cells (HBL6, JSC-PEL, BC2 and BC3), EBV-infected Burkitt's lymphoma cells (IB4, B98-5, Akata and Raji), EBV-negative Burkitt's lymphoma cells (DG75) and CMV-infected HEL cells were used as DNA templates for individual PCR amplification reactions using the sets of primers listed in Table 1. The viral gene products of the individual PCR reactions were confirmed by gel electrophoresis to ensure correct length of the target fragments and to confirm the presence of viral genome within the specified cells. KSHV-positive BC2, BC3, HBL6 and JSC-PEL cells showed correct 346-bp fragments for KSHV LANA; EBV-positive Raji, B98-5, IB4 and Akata cells showed correct 167-bp fragments for EBV EBER1; HCMV-positive HEL cells showed correct 347-bp fragments for HCMV IE; and EBV/KSHV/CMV-negative DG75 cells failed to produce any fragment at all (Fig. 2B). Thus, no non-specific products were at all detected in all PCR reactions, which demonstrated the high specificities of primer sets for viral genes.

The KSHV LANA, EBV EBER1 and HCMV IE genes were subcloned into the pGEM-T plasmid vectors to ensure accurate dispensation of viral gene copy numbers as PCR

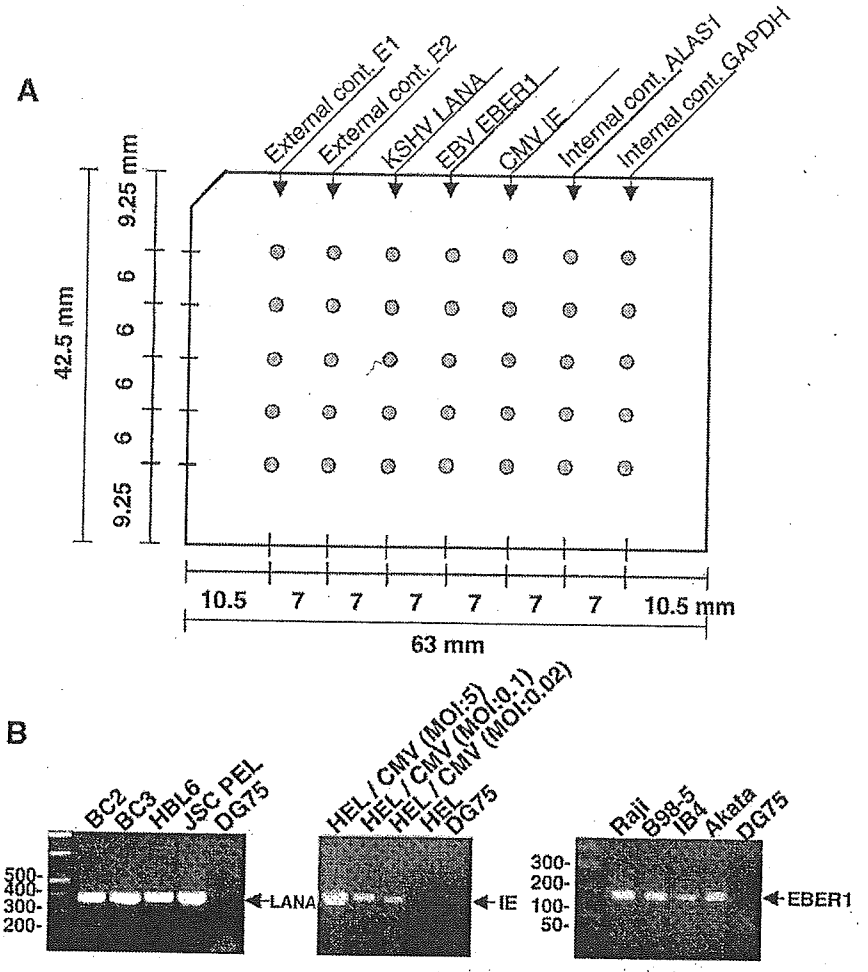

Fig. 2. (A) Schematic diagram showing the positions of the immobilized probes spotted in quintuplicate on a nylon membrane. (B) Amplification of viral target genes with designed primer sets from genomic DNA of infected cell lines. LANA, EBER1 and IE genes were amplified from KSHV positive PEL cells (HBL6, JSC PEL, BC2 and BC3), EBV-positive Burkitt's lymphoma cells (IB4, Akata and Raji) and HEL cells infected with CMV (Towne strain) at a MOI of 0.02, 0.1 and 5. DG75 cells, herpesvirus-negative B lymphoma cells, were used along with uninfected HEL cells as negative control.

templates for sensitivity test (1 viral gene-containing plasmid approximates one viral genome copy). We then tested the efficacy of the DNA array by hybridizing multiplex PCR products of viral gene-containing plasmids onto the DNA array for detection. We mixed 1×10^3 copies of viral gene-containing pGEM-T plasmid for each herpesvirus with 5 copies of external control plasmid as multiplex PCR templates and performed three separate multiplex PCR reactions (one for each virus) with appropriate primer sets listed in Table 1 in the presence of biotinylated dUTP and dNTP-(minus-dTTP). Internal controls were not used since no genomic DNA was present. Subsequently, the biotinylated multiplex PCR products for each virus were hybridized to three different DNA arrays containing DNA probes for all three human herpesviruses and external controls, and we found no cross-reactivity of any one virus against two other viruses in the same DNA array (Fig. 3). The signals of the amplified PCR products were highly specific for the respective target virus detection lanes, and in addition, equal hybridization intensities were observed in all five spots of the same lane on the array. These results indicate that our multiplex PCR/DNA array approach is highly specific for detection of different viruses belonging to the same herpesvirus family.

Sensitivity of PCR-based array hybridization

One main advantage of DNA array-based pathogen detection method is thought to be high sensitivity. To evaluate the threshold of detection by DNA array in our assay, four 10-fold serial dilutions of the viral DNA plasmids (i.e., 10^3, 10^2, 10^1 and 10^0 copies of each viral gene-containing plasmid) were used as different multiplex PCR templates with the same primer sets (three virus-specific primer pairs plus four control primer pairs including both the external and internal controls), and all three viral gene-containing plasmids of the same dilution factors were mixed together and subjected to a single multiplex PCR reaction (a total of four multiplex PCR reactions for four different dilution factors) (Fig. 4). Quantitative analysis data of the mean chemiluminescent signal intensities from all five spotted dots on the DNA array are shown in Fig. 4E: the arrow indicates the minimal threshold of detection for the chemiluminescence imager from noise, and therefore, any signal below the threshold

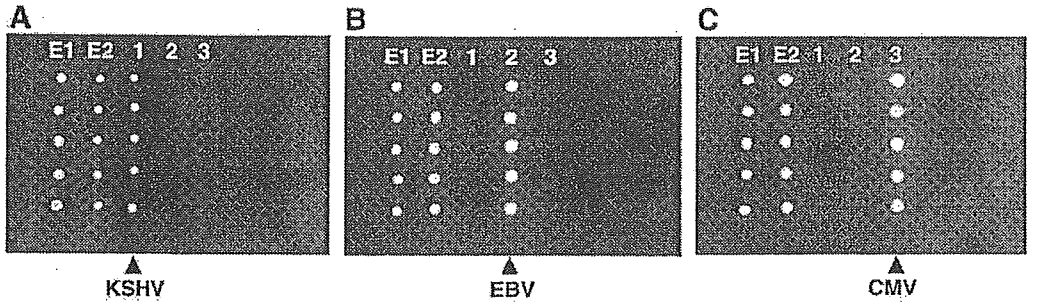

Fig. 3. Hybridization patterns of amplified PCR products by multiplex PCR using viral gene-containing plasmids for KSHV LANA (A), EBV EBER1 (B) and CMV IE (C) as templates with external control plasmid templates E1 and E2. No internal controls were used in these experiments. Amplicons were hybridized to DNA array membrane. Each column consisted of 5 dotted spots, which are specific for hybridization with LANA PCR products (column 1), EBRE1 products (column 2), IE products (column 3) and external controls (columns E1 and E2). Array membranes were processed with the Phototope-Star detection kit, and the chemiluminescent signals were visualized by Fluor-S MAX2 Multi Imaging System. The arrowhead indicates the signal specificity threshold of the imager.

of detection would be regarded as a non-specific signal. We found that the DNA array is extremely sensitive, and that the threshold of detection for EBV EBER1 requires only 100 copies of the viral gene-containing plasmid (Fig. 4B). In addition, it was found that KSHV LANA or CMV IE PCR product with only 1 copy of the viral gene-containing plasmid as template is detectable on the DNA array (Fig. 4D). Thus, these results indicate that multiplex PCR-based DNA array hybridization test is extremely sensitive.

In the case of EBV, it can be inferred that the shorter length of the PCR fragment of EBER1 gene (167 bp) may have incorporated less biotinylated dUTP in comparison with the KSHV and CMV fragments which are twice longer than the EBV fragment. Therefore, due to the presence of less biotinylated dUTP, which yields lower signal intensity, the threshold of detecting the 167-bp EBV fragment would be 100-fold higher than those of CMV and KSHV. A new EBV target sequence with a similar length to those of KSHV and CMV target gene products should be used to increase the detection sensitivity to 1 copy of EBV genome.

Real-time detection of herpesvirus in virus-infected B lymphoblastoid and fibroblast cells

To address the question of whether our developed assay system has a diagnostic value for epidemiological and clinical

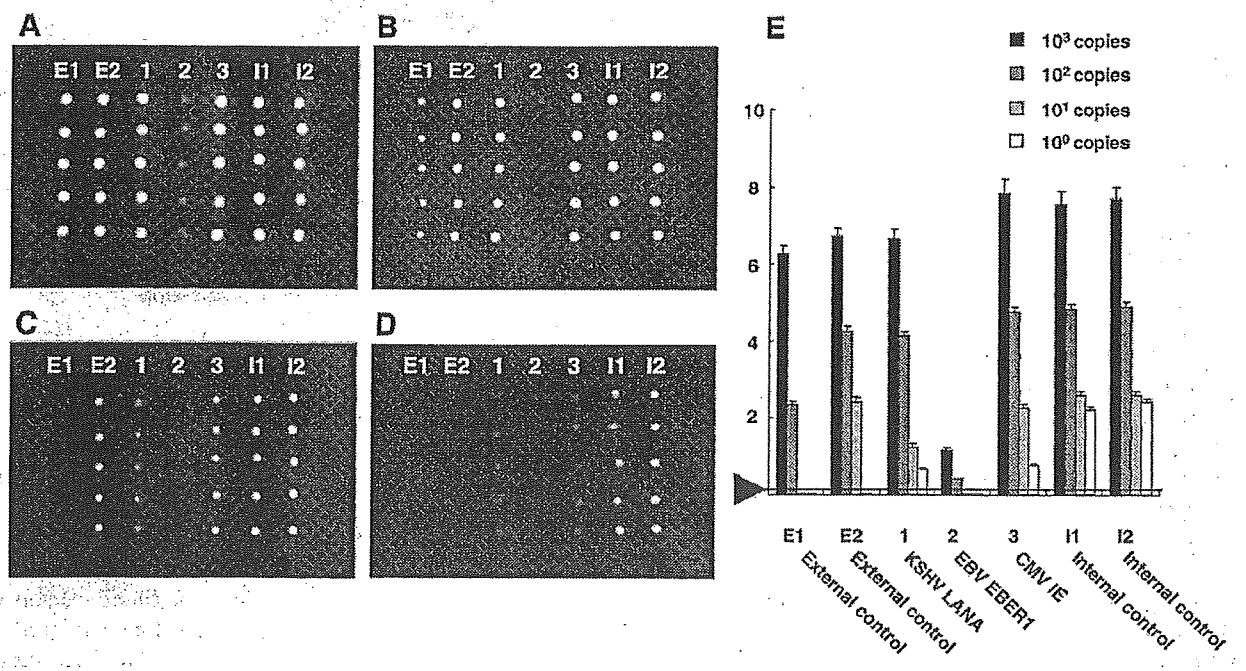

Fig. 4. Sensitivity of detection by DNA array using different DNA copy numbers as templates. Ten-fold serially diluted template plasmids containing subcloned viral genes were mixed with external control plasmids and were subjected to multiplex PCR amplifications with specific primers. PCR template copy numbers of 1×10^3 (A), 1×10^2 (B), 1×10^1 (C) and 1×10^0 (D) were used for all viruses. PCR templates with the same dilution factor from LANA, EBER1 and IE plasmids were mixed together in the presence of external control plasmids and were then subjected to multiplex PCR reaction. Quantitation of hybridization signals is shown in panel E. The arrow in panel E indicates the signal specificity threshold of the imager. Each bar represents the mean fluorescent signal intensity from 5 spots of the same viral detection lane. The error bar indicates the standard deviations.

studies, we utilized known KSHV- and/or EBV-infected B lymphoblastoid cells isolated from patients suffering from immunodeficiency-associated primary effusion lymphoma and Burkitt's lymphoma, as well as HEL cells primarily infected with CMV, to detect viral DNA by multiplex PCR-based DNA array hybridization (Fig. 5). Total genomic DNAs harvested from these cells were mixed with primers specific for KSHV LANA, EBV EBER1 and CMV IE genes, and multiplex PCR was performed in the presence of biotinylated dUTP. Amplified viral gene fragments labeled with biotin were then hybridized to specific KSHV, EBV and CMV DNA probes immobilized on the DNA array membrane.

Primary effusion lymphoma cells (BC2) are double infected with both KSHV and EBV, and the multiplex PCR products specific for both viruses were accurately detected in these cells by our assay system (Fig. 5A). Another primary effusion lymphoma cells (BC3) are infected only with KSHV, and the DNA arrays gave positive signals only for KSHV and negative ones for EBV (Fig. 5B). EBV-infected Burkitt's lymphoma cells, Raji and Akata cells, both yielded positive signals specific for EBV on the DNA arrays (Figs. 5C and D, respectively). HEL cells infected with CMV at a MOI of 1 and 10 both showed positive signals specific for CMV on the DNA arrays (Figs. 5E and F, respectively). Thus, these results show that our test is highly specific and sensitive, and that no cross-hybridization among different target probes is at all observed, indicating that our detection system is applicable for the use as a diagnostic tool. It should be noted that hybridization signals of internal control (I1) and external control (E1) were not observed in HEL cells (Fig. 5). It is possible that the ALAS1 gene, I1 internal control gene, may have been selectively methylated in HEL cells. With respect to low signal of E1, it is possible that the large amount of total genomic DNA templates used for the multiplex PCR may have affected the efficiency of amplifying the external plasmid with the primers designed for the external control, which might be meant for very stringent PCR conditions for E1 but less stringent PCR conditions for genomic gene products. Anyhow, internal control I2 and external control E2 can work very well in our assay, and therefore, these two genes will be used as the only internal and external controls, respectively, for future diagnostic applications.

In this study, we have developed the multiplex PCR-based DNA array hybridization assay that is capable of simultaneously detecting all three lymphotropic herpesviruses from a single cell sample with excellent specificity and sensitivity. In our assay, the target viral genes were chosen because they encode important proteins functioning in viral pathogenesis, and their sequences are highly conserved across substrains of the same herpesvirus. Our developed assay allows for the detection of 1 copy of KSHV and CMV genomes and 100 copies of EBV genome. Although other groups have also developed the PCR-based DNA array methods for human herpesviruses, their methods need 10 to 100 more copies of the templates than those required in our method (Foldes-Papp et al., 2004; Striebel et al., 2004; Boriskin et al., 2004).

Initial symptoms of herpesvirus infection, especially CMV, in immunosuppressed patients typically include fever, headache, cough and malaise, which are almost indistinguishable from hospital-acquired *Streptococcus pneumoniae* infections. The delay in diagnosing herpesvirus infection often has devastating consequences such as CMV encephalitis, therapy-resistant pneumonia and graft rejection in transplant recipients (Fishman

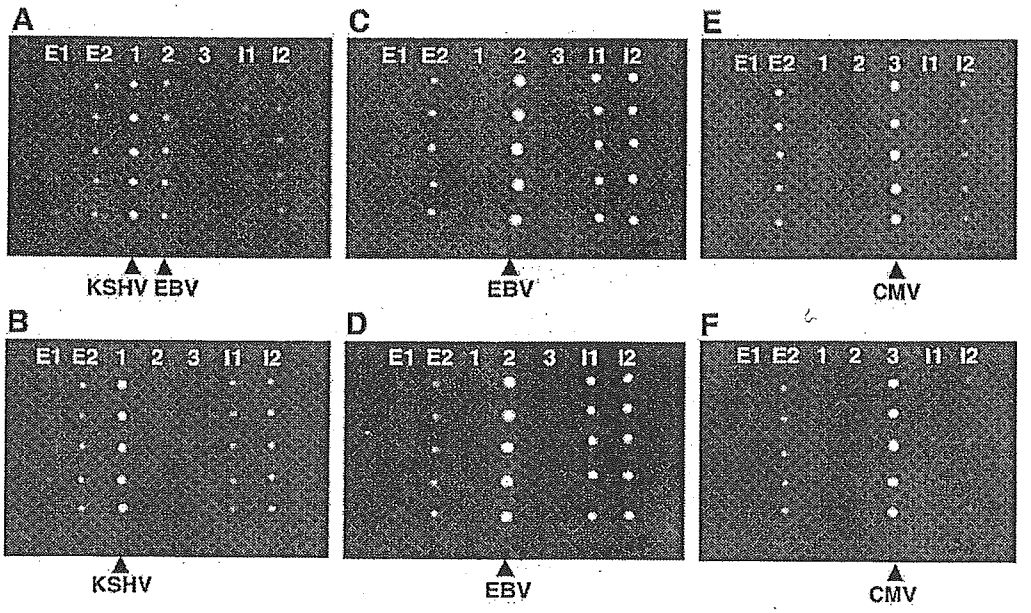

Fig. 5. Detection of virus genomic DNA in the virus-infected cells isolated from patients. Genomic DNAs were prepared from KSHV and EBV double-positive PEL, BC2 cells (A), KSHV-positive PEL, BC3 cells (B), EBV-positive Raji cells (C), EBV-positive Akata cells (D) and HEL cells infected with CMV (Towne strain) at a MOI of 1 (E) and 10 (F). Target LANA, EBER1 and IE genes were amplified from genomic DNA via multiplex PCR reaction in the presence of biotinylated dUTP, and the PCR products were hybridized to DNA array nylon membrane in which KSHV, EBV and CMV DNA probes were immobilized. The arrowhead indicates the specific virus signal.

Neuropathology 2005; **25**, 388–394

Workshop: Recent Advances in Motor Neuron Disease

Golgi apparatus of the motor neurons in patients with amyotrophic lateral sclerosis and in mice models of amyotrophic lateral sclerosis

Yukio Fujita and Koichi Okamoto

Department of Neurology, Gunma University Graduate School of Medicine, Maebashi, Gunma, Japan

We examined the Golgi apparatus (GA) of motor neurons of patients with ALS and in mice models of ALS by immunohistological method using antiserum against MG160 and against components of the trans-Golgi network (TGN46). The GA of half of the remaining spinal cord motor neurons of patients with sporadic ALS showed fragmentation, where the GA were dispersed or fragmented into numerous small, isolated elements. The GA of Betz cells in sporadic ALS were fragmented similar to that of anterior horn cells, and the GA of spinal cord motor neurons of those with familial ALS and of those with ALS with basophilic inclusions were fragmented or diminished. The GA in the majority of the motor neurons contained Bunina bodies, basophilic inclusions and superoxide dismutase 1 (SOD1)-positive aggregates were fragmented. The motor neurons in transgenic mice expressing G93A mutation of the *SOD1* gene showed the fragmentation of the GA months before the onset of paralysis. These findings suggest that the fragmentation of GA may be related to the neuronal degeneration in patients with ALS.

Key words: amyotrophic lateral sclerosis, Golgi apparatus, MG160, motor neuron disease.

INTRODUCTION

ALS is a chronic degenerative disease characterized by the progressive degeneration and loss of motor neurons in the spinal cord, brainstem and motor cortex.[1] The etiology of the sporadic form of ALS, representing approximately 90% of all cases, is unknown, whereas a significant percentage of familial ALS is caused by mutations of the gene that transcribes the enzyme Cu, Zn superoxide dismutase 1 (SOD1).[2]

The Golgi apparatus (GA) plays a role in the transport, processing and targeting of numerous proteins destined for secretion, plasma membrane and lysosomes.[3,4] In neurons, the GA is involved in the axoplasmic flow of endogenous proteins and of exogenous macromolecules transported by orthograde, retrograde and transsynaptic routes.[5–7] Lesions of the neuronal GA undoubtedly have detrimental consequences for the function of axon and presynaptic terminals. The MG160 protein is a conserved sialoglycoprotein present as part of the medial cisternae of the GA.[8] Antiserum generated against immunoaffinity purified MG160 has proven to be a reliable and sensitive marker of the GA for many species, including humans.[8,9] The application of this antiserum to sporadic ALS and asymptomatic and paralyzed transgenic mice expressing the G93A mutation of *SOD1* led to the detection of an unusual "lesion" of the GA of spinal cord motor neurons.[8–16] This "lesion" consists of dispersion of the normal network of large and irregular elements of the GA into numerous small, disconnected elements, suggesting that the organelle is fragmented. The recognition of fragmented GA in asymptomatic transgenic mice expressing the G93A mutation of *SOD1* suggests that the GA is an early target of the pathological process which initiates neuronal degeneration. We show here that fragmentation of the GA of the motor neurons occurs in ALS, in other motor neuron diseases (MND) and in mice models of ALS. We also reveal that the GA of a majority of motor neurons that contain inclusions, such as Bunina bodies, basophilic inclusions and SOD1-positive aggregates, are fragmented in ALS/MND. These results indicate that the fragmentation of GA may be related to the neuronal degeneration in patients with ALS/MND, and also indicate

Correspondence: Yukio Fujita, MD, PhD, Department of Neurology, Gunma University School of Medicine, 3-39-22, Showa-machi, Maebashi, Gunma 371-8511, Japan. Email: yfujita@showa.gunma-u.ac.jp

Received 30 November 2004; revised and accepted 15 December 2004.

that the intracytoplasmic inclusions in ALS/MND may be associated with the fragmentation of GA.

MATERIALS AND METHODS

Tissues of ALS/MND were obtained during autopsy and were then fixed in phosphate-buffered formalin and embedded in paraffin. Transgenic mice expressing the G93A mutation of the *SOD1* gene were obtained from the Jackson Laboratory, and were made available by M.E. Gurny, who initially developed the first transgenic animal model of ALS.[17] Spinal cords and brainstems of the transgenic and control mice from 8 to 19 weeks of age were fixed by perfusion and immersion in 4% paraformaldehyde, after which they were embedded in paraffin.

Five-micrometer-thick deparaffinized sections from ALS/MND patients including 16 cases of sporadic ALS,[18] two cases of juvenile ALS with basophilic inclusions,[19,20] three cases of familial ALS with *SOD1* mutations and posterior column involvement,[21,22] five cases of X-linked spinal and bulbar muscular atrophy,[23] and from 20 transgenic mice expressing the G93A mutation of *SOD1* were immunostained with a polyclonal anti-MG160 antibody (1:1000 dilution), which recognizes a sialoglycoprotein of the medial cisternae of the GA,[8,9] and a polyclonal anti-TGN46 antibody[24] (1:4000 dilution), which recognizes an intrinsic membrane protein of the trans-Golgi network (TGN). These antibodies were used as markers for the GA. We also immunostained the motor neurons with monoclonal 1C2 antibody (Chemicon, Temecula, CA, USA; 1:10 000 dilution), which recognizes a polyglutamine stretch, and polyclonal SOD1 (Cu, Zn) antibody (Carbiochem, San Diego, CA, USA; 1:2000 dilution).

RESULTS

Anterior horn cells and Betz cells in ALS

The GA of motor neurons, including the anterior horn cells and Betz cells, were specifically immunostained with anti-MG160 and anti-TGN46 antiserum, and the immunohistological findings were almost similar between the two at the light microscopy level. The normal GA of the motor neurons had a larger, angular or elongated profile which filled the cell body and extended into the proximal segments of the dendrites (Fig. 1). Over 50% of the GA in the remaining anterior horn cells of the patients with ALS and ALS with dementia were fragmented, for which the GA lost its normal network-like configuration and which was replaced by numerous disconnected elements (Fig. 1). Few fragmented GA were found in the controls. The GA of the majority of anterior horn cells containing Bunina bodies were fragmented,[12] and fragmented GA were also

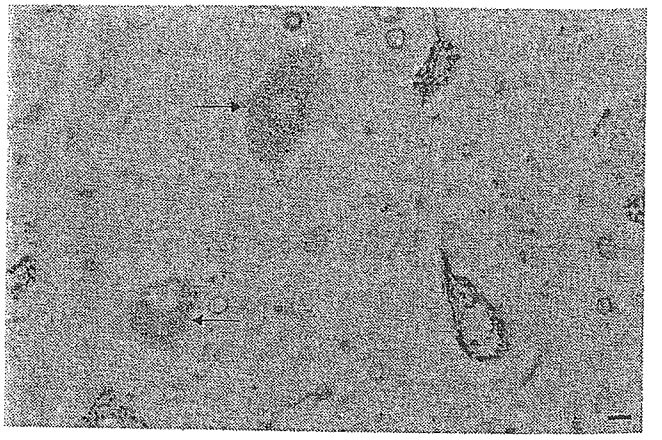

Fig. 1 Immunostaining of anterior horn cells in a patient with sporadic ALS. MG160 immunostaining shows neurons with a normal Golgi apparatus (GA) network and fragmented GA (arrows). Bar, 20 μm.

Fig. 2 Immunostaining of the neurons of hypoglossal nerve nucleus from a patient with sporadic ALS. MG160 immunostaining shows a fragmented Golgi apparatus (arrow), which was identical to that found in anterior horn cells. Bar, 20 μm.

seen in the hypoglossal nuclei (Fig. 2). Twelve of the 16 ALS patients contained 2–50% fragmented GA, and 42 of 317 (13.2%) examined Betz cells showed fragmentation of the GA (Fig. 3).[18] However, only three of 472 (0.6%) Betz cells exhibited fragmentation of the GA in 10 non-ALS patients.[18] The frequency of fragmentation varied, but the number of Betz cells was markedly reduced for the ALS patients, and therefore we could not assess the relationship between the frequency of fragmented GA in the Betz cells and the clinical course of the disease with respect to the age of onset, duration of illness and pyramidal tract signs.[18]

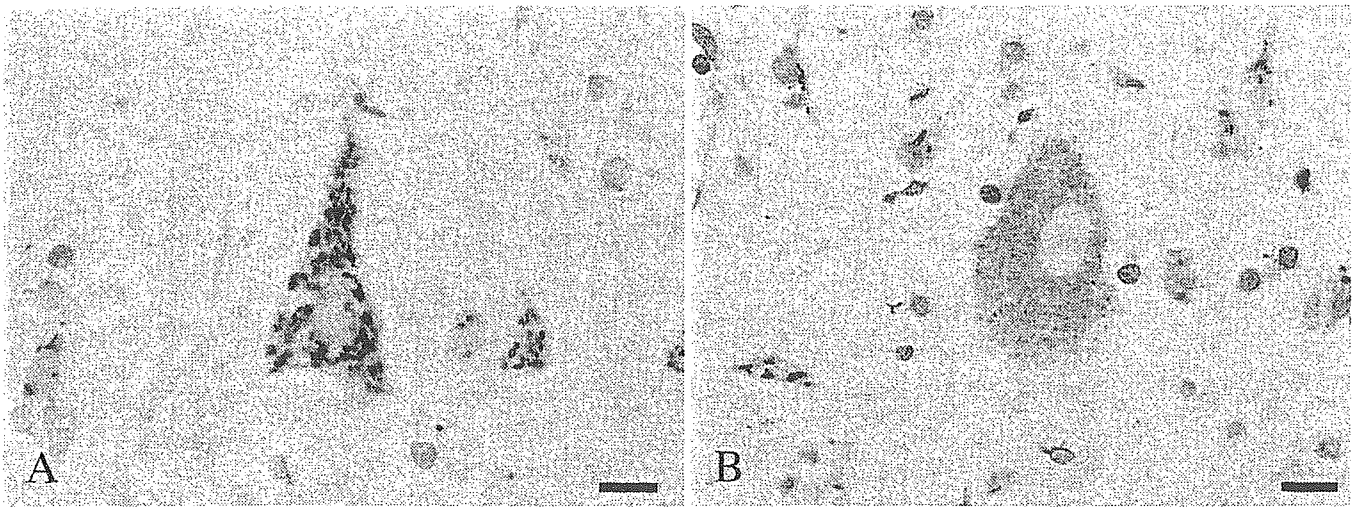

Fig. 3 Immunostaining of Betz cells in a patient with sporadic ALS. MG160 immunostaining shows Betz cells with (A) a normal Golgi apparatus (GA) network and (B) fragmented GA. Bars (A,B) 40 μm.

Fig. 4 Immunostaining of anterior horn cells from a patient with juvenile ALS with basophilic inclusions. MG160 immunostaining shows two anterior horn cells with (left) a normal Golgi apparatus (GA) network and (right) fragmented GA. Basophilic inclusion denoted by the arrow was not stained by anti-MG160 antibody. All anterior horn cells containing the inclusions showed fragmentation or reduced number of the GA. Bar, 20 μm.

Juvenile ALS with basophilic inclusions

The GA of the anterior horn cells were adequately and specifically immunostained with the anti-MG160 antiserum. Sixty per cent of the preserved large motor neurons showed fragmentation of the GA,[19] and all neurons containing the inclusions showed fragmentation and reduced numbers of GA (Fig. 4).[19] Fragmentation of the GA was identical to that previously reported for motor neurons of the spinal cord and motor cortex of ALS patients.

Familial ALS with *SOD1* mutations and posterior column involvement

The large motor neurons of spinal cords of patients with familial ALS with *SOD1* mutation and posterior column involvement were markedly reduced in number, for which detailed neuropathological findings were already previously reported.[21,25,26] The GA of the neurons in the anterior horn cells were adequately and specifically immunostained with anti-MG160 antiserum, and the GA of small neurons showed almost normal profiles (Fig. 5).[22] However, 10 of 14 preserved large motor neurons in seven transverse sections of spinal cords from three patients showed fragmentation and reduced numbers of GA (Fig. 5).[22] For large neurons that contained SOD1-positive aggregates, the fragmented GA was not strongly stained compared to normal GA, and had accumulated around the nuclei (Fig. 5).

Motor neurons from transgenic mice expressing the G93A mutation of the *SOD1* gene

Transgenic mice expressing the G93A mutation of the *SOD1* gene showed the microvesiculation of the anterior horn cells and small SOD1-positive aggregates in the neuropil of spinal cords from 8 weeks of age. The mice also had fragmented GA in anterior horn cells and motor neurons in the brainstem from 8 weeks of age (Fig. 6), and the GA of almost all of the motor neurons that contained SOD1-positive aggregates showed fragmentation or were diminished. It is important to note that fragmentation of the GA was present as early as 8 weeks of age, the earliest time-point examined, which was before the first signs of clinical dysfunction were apparent.

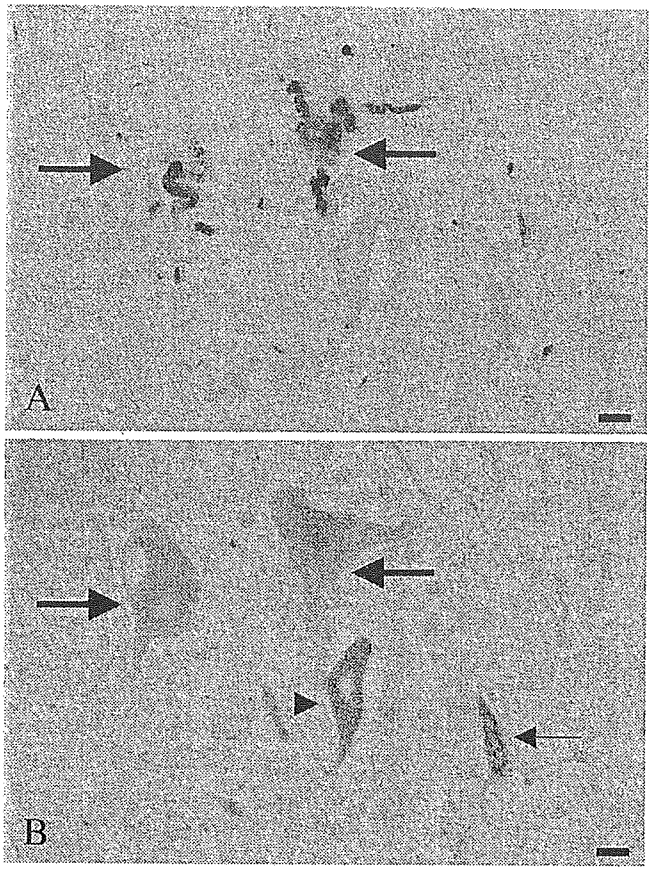

Fig. 5 (A) superoxide dismutase 1 (SOD1; Cu, Zn) immunostaining of anterior horn cells from a patient with familial ALS with *SOD1* mutation and posterior column involvement. SOD1-positive aggregates were observed in two large anterior horn cells as denoted by the arrows. Bar, 20 μm. (B) MG160 immunostaining of the same section as in (A). A small anterior horn cell shows a normal Golgi apparatus (GA) network as indicated by the small arrow, but two large ones containing SOD1-positive aggregates show fragmentation and reduced number of the GA (large arrows); the other middle one denoted by the arrowhead shows fragmentation. Bar = 20 μm.

X-linked spinal and bulbar muscular atrophy

The GA of residual motor neurons was normal or reduced in size.[23] However, the profiles of small or atrophic GA were different from those of the fragmented GA. Fragmentation of the GA was previously observed only in a few anterior horn cells,[23] and double immunostaining using anti-MG160 and 1C2 antibodies showed that anterior horn cells bearing an intranuclear inclusion had a normal (Fig. 7) or atrophic GA.[23] Fragmentation of the GA was not observed in neurons bearing an intranuclear inclusion.

DISCUSSION

The fragmentation of GA were frequently observed in the motor neurons in patients with sporadic ALS, familial ALS with posterior column involvement and juvenile ALS with basophilic inclusions. In addition, all mice expressing the G93A mutation of the *SOD1* gene showed fragmentation of the GA in anterior horn cells and motor neurons in the brainstem. It is important to note that fragmentation of the GA was present as early as 8 weeks of age, the earliest time-point examined, which was before the first signs of clinical dysfunction were noted. It is unlikely that fragmentation of the GA is an artifact of post-mortem autolysis for several reasons, one being that other groups of neurons, such as adjacent neurons of the column of Clarke, did not exhibit fragmentation of the GA.[11]

In the Betz cells, the immunohistological configuration of the normal and fragmented GA was identical to that of anterior horn cells.[8–16] However, the number of Betz cells with fragmented GA (13.2% for patients with ALS in contrast to 0.6% for the non-ALS controls) was lower than that observed in the spinal cord motor neurons. This may be due to the severe loss of Betz cells in patients with ALS, and suggests that the same mechanism is responsible for fragmentation of the GA in Betz cells and anterior horn cells, although the time-course of the pathological changes for these two groups of neurons may differ.

Aggregation of mutant SOD1 in 13-nm filaments, ubiquitin-positive inclusions and fragmentation of the GA are correlated with the progression of disease in transgenic mice expressing mutant SOD1.[27] Furthermore, we found that 10 of 14 preserved large motor neurons in seven transverse spinal cord sections from three patients with familial ALS with *SOD1* mutation and posterior column involvement showed fragmentation and reduced GA. In addition, in large neurons that contained SOD1-positive aggregates the fragmented GA was not strongly stained compared to normal GA, and the fragments had accumulated around the nuclei. Fragmentation of GA also occurs in a majority of motor neurons that contain Bunina bodies or basophilic inclusions in patients with ALS.[12,19] However, an immunohistological study showed that the GA is not fragmented in nigral neurons containing Lewy bodies in patients with Parkinson's disease (Y. Fujita and K. Okamoto, unpublished data 2005). Therefore, in patients with ALS/MND, abnormal proteinaceous cytoplasmic aggregates may be related to the fragmentation of GA. The precise molecular mechanisms linking the aggregation of proteins and fragmentation of the GA are not known, and the identification of the molecular composition of the aggregated proteins present in patients with sporadic ALS with a variety of inclusions remains a major challenge.

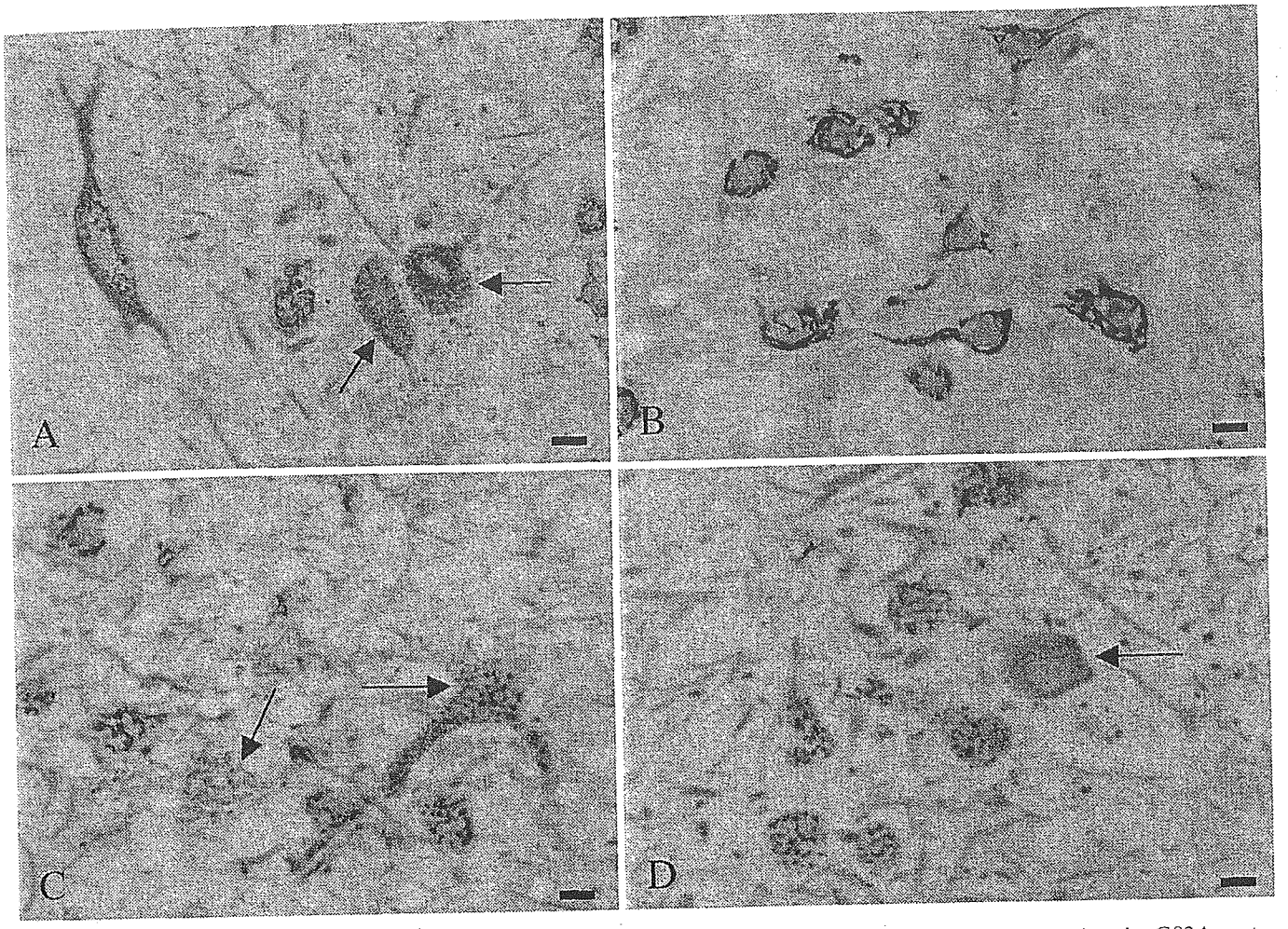

Fig. 6 MG160 immunostaining of spinal cord and brainstem motor neurons in transgenic (Tg) mice expressing the G93A mutation of the *SOD1* gene. (A) Fragmentation of the Golgi apparatus (GA) was seen as denoted by the arrows in a spinal cord section from a Tg mouse at 19 weeks of age. (B) No fragmented GA were seen in the neurons of fascial nerve nucleus of a control mouse at 15 weeks of age. (C) Fragmentation of the GA were seen in the fascial nerve nucleus from a Tg mouse at 15 weeks of age. (D) Fragmentation and reduced GA content was seen in the trigeminal nerve nucleus of a Tg mouse at 15 weeks of age. Bars (A–D) 20 μm.

Fragmentation of the GA is not specific for ALS, because similar findings have also been observed in the spinal cord motor neurons of patients with mitochondria myopathy,[13] olivary hypertrophic neurons[28] and ballooned neurons in those with corticobasal degeneration and CJD.[24] Experimental evidence of cell injury induced by a variety of agents indicates that fragmentation of the GA is associated with defects of membrane flow and protein transport.[29–32] We show here that the GA of motor neurons were frequently fragmented in patients with ALS/MND and the majority of motor neurons that contained cytoplasmic inclusions had the fragmented GA. Furthermore, the fragmentation of GA is one of the early neuropathological changes in transgenic mice expressing the G93A mutation of the *SOD1* gene. These results suggest that the fragmentation of GA may be related to the neuronal degeneration in patients with ALS/MND, and further examinations about the significance of the fragmentation of the GA are required.

ACKNOWLEDGMENTS

This work was presented at the 45th Annual Meeting of the Japanese Society of Neuropathology, May 27, 2004, Maebashi, Japan.

We are deeply grateful to N.K. Gonatas for donating anti-MG160 antibody, and to Professor H. Kusaka, H. Aizawa, B. Mihara, M. Yaguchi and Professor A. Hirano for their donation of valuable tissues.

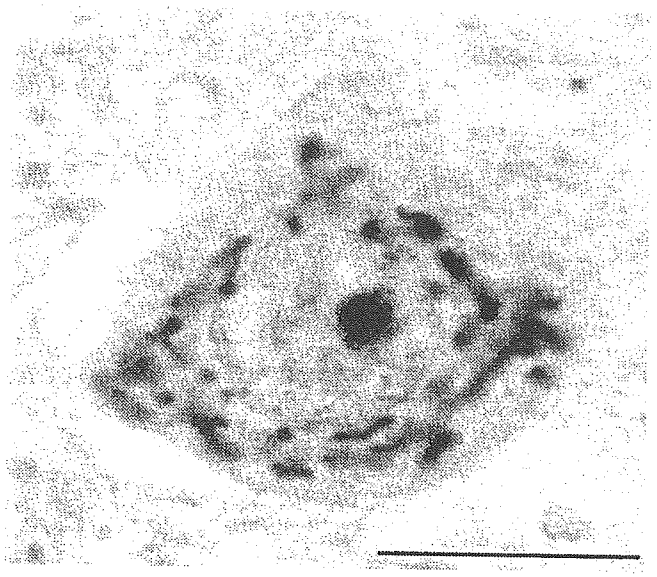

Fig. 7 An anterior horn cell double-immunostained with 1C2 antibody and MG-160 antibody from a case of X-linked spinal and bulbar muscular atrophy. A neuron containing an intranuclear inclusion shows a normal Golgi apparatus network. Bar, 20 μm.

This work was supported by a grant to K. Okamoto from the Ministry of Health, Labour and Welfare, Japan.

REFERENCES

1. Hirano A. Neuropathology of ALS: an overview. *Neurology* 1996; **47** (Suppl. 2): S63–66.
2. Rosen DR, Siddique T, Patterson D *et al.* Mutations in Cu/Zn superoxide dismutase gene are associated with familial amyotrophic lateral sclerosis. *Nature* 1993; **362**: 59–62.
3. Farquhar MG. Progress in unraveling pathways of Golgi traffic. *Annu Rev Cell Biol* 1985; **1**: 447–488.
4. Mellman I, Simons K. The Golgi complex: in vitro veritas? *Cell* 1992; **68**: 829–840.
5. Hammerschlag R, Stone GC, Bolen FA, Lindsay JD, Ellisman MH. Evidence that all newly synthesized proteins destined for fast axonal transport pass through the Golgi apparatus. *J Cell Biol* 1982; **93**: 568–575.
6. Rhodes CH, Stieber A, Gonatas NK. A quantitative electron microscopic study of the intracellular localization of wheat germ agglutinin in retinal neurons. *J Comp Neurol* 1986; **254**: 287–296.
7. Rhodes CH, Stieber A, Gonatas NK. Transneuronally transported wheat germ agglutinin labels glia as well as neurons in the rat visual system. *J Comp Neurol* 1987; **261**: 460–465.
8. Gonatas JO, Mezitis SGE, Stieber A, Fleischer B, Gonatas NK. MG-160: a novel sialoglycoprotein of the medial cisternae of the Golgi apparatus. *J Biol Chem* 1989; **264**: 646–653.
9. Croul S, Mezitis SGE, Stieber A *et al.* Immunocytochemical visualization of the Golgi apparatus in several species, including human, and tissues with an antiserum against MG-160, a sialoglycoprotein of rat Golgi apparatus. *J Histochem Cytochem* 1990; **38**: 957–963.
10. Mourelatos Z, Gonatas NK, Stieber A, Gurney ME, Dal Canto MC. The Golgi apparatus of spinal cord motor neurons in transgenic mice expressing mutant Cu, Zn superoxide dismutase becomes fragmented in early, preclinical stages of the disease. *Proc Natl Acad Sci USA* 1996; **93**: 5472–5477.
11. Mourelatos Z, Yachnis A, Rorke L, Mikol J, Gonatas NK. The Golgi apparatus of motor neurons in amyotrophic lateral sclerosis. *Ann Neurol* 1993; **33**: 608–615.
12. Stieber A, Chen Y, Wei S *et al.* The fragmented neuronal Golgi apparatus in amyotrophic lateral sclerosis includes the trans-Golgi-network: functional implications. *Acta Neuropathol (Berl)* 1998; **95**: 245–253.
13. Gonatas NK, Stieber A, Mourelatos Z *et al.* Fragmentation of the Golgi apparatus of motor neurons in amyotrophic lateral sclerosis. *Am J Pathol* 1992; **140**: 731–737.
14. Gonatas NK. Contributions to the physiology of the Golgi apparatus. *Am J Pathol* 1994; **145**: 751–761.
15. Mourelatos Z, Adler H, Hirano A, Donnenfeld H, Gonatas JO, Gonatas NK. Fragmentation of the Golgi apparatus of motor neurons in amyotrophic lateral sclerosis revealed by organelle-specific antibodies. *Proc Natl Acad Sci USA* 1990; **87**: 4393–4395.
16. Mourelatos Z, Hirano A, Rosenquist AC, Gonatas NK. Fragmentation of the Golgi apparatus of motor neurons in amyotrophic lateral sclerosis (ALS). Clinical studies in ALS of Guam and experimental studies in deafferented neurons and in β, β' iminodipropionitrile axonopathy. *Am J Path* 1994; **144**: 1288–1300.
17. Gurney ME, Pu H, Chiu AY *et al.* Motor neuron degeneration in mice that express a human Cu, Zn superoxide dismutase mutation. *Science* 1994; **264**: 1772–1775.
18. Fujita Y, Okamoto K, Sakurai A, Amari M, Nakazato Y, Gonatas NK. Fragmentation of the Golgi apparatus of Betz cells in patients with amyotrophic lateral sclerosis. *J Neurol Sci* 1999; **163**: 81–85.
19. Fujita Y, Okamoto K, Sakurai A, Kusaka H, Aizawa H, Mihara B, Gonatas NK. The Golgi apparatus is fragmented in spinal cord motor neurons of amyotrophic lateral sclerosis with basophilic inclusions. *Acta Neuropathol (Berl)* 2002; **103**: 243–247.
20. Aizawa H, Kimura T, Hashimoto K, Yahara O, Okamoto K, Kikuchi K. Basophilic cytoplasmic inclusions

in a case of sporadic juvenile amyotrophic lateral sclerosis. *J Neurol Sci* 2000; **176**: 109–113.

21. Shibata N, Hirano A, Kobayashi M *et al.* Intense superoxide dismutase-1 immunoreactivity in intracytoplasmic hyaline inclusions of familial amyotrophic lateral sclerosis with posterior column involvement. *J Neuropathol Exp Neurol* 1996; **55**: 481–490.
22. Fujita Y, Okamoto K, Sakurai A, Gonatas NK, Hirano A. Fragmentation of the Golgi apparatus of the anterior horn cells in patients with familial amyotrophic lateral sclerosis with SOD1 mutations and posterior column involvement. *J Neurol Sci* 2000; **174**: 137–140.
23. Yaguchi M, Hashizume Y, Yoshida M, Gonatas NK, Okamoto K. Reduction of the size of the Golgi apparatus of spinal anterior horn cells in patients with X-linked spinal and bulbar muscular atrophy. *ALS Other MND* 2003; **4**: 17–21.
24. Sakurai A, Okamoto K, Fujita Y *et al.* Fragmentation of the Golgi apparatus of the ballooned neurons in patients with corticobasal degeneration and Creutzfeldt-Jakob disease. *Acta Neuropathol* 2000; **100**: 270–274.
25. Hirano A, Nakano I, Kurland LT, Mulder DW, Holley PW, Saccomanno G. Fine structural study of neurofibrillary changes in a family with amyotrophic lateral sclerosis. *J Neuropathol Exp Neurol* 1984; **43**: 471–480.
26. Kato T, Hirano A, Kurland LT. Asymmetric involvement of the spinal cord involving both large and small anterior horn cells in a case of familial amyotrophic lateral sclerosis. *Clin Neuropathol* 1987; **6**: 67–70.
27. Stieber A, Gonatas JO, Gonatas NK. Aggregation of ubiquitin and a mutant ALS-linked SOD1 protein correlate with disease progression and fragmentation of the Golgi apparatus. *J Neurol Sci* 2000; **173**: 53–62.
28. Takamine K, Okamoto K, Fujita Y, Sakurai A, Takatama M, Gonatas NK. The involvement of the neuronal Golgi apparatus and trans-Golgi network in the human olivary hypertrophy. *J Neurol Sci* 2000; **182**: 45–50.
29. Cao H, Thompson HM, Krueger EW, McNiven MA. Disruption of Golgi structure and function in mammalian cells expressing a mutant dynamin. *J Cell Sci* 2000; **113**: 1993–2002.
30. Cole NB, Sciaky N, Marotta A, Song J, Lippincott-Schwartz J. Golgi dispersal during microtubule disruption: regeneration of Golgi stacks at peripheral endoplasmic reticulum exit sites. *Mol Biol Cell* 1996; **7**: 631–650.
31. Dascher C, Balch WE. Dominant inhibitory mutants of ARF1 block endoplasmic reticulum to Golgi transport and trigger disassembly of the Golgi apparatus. *J Biol Chem* 1994; **269**: 1437–1448.
32. Wilson BS, Nuoffer C, Meinkoth JL *et al.* A Rab1 mutant affecting guanine nucleotide exchange promotes disassembly of the Golgi apparatus. *J Cell Biol* 1994; **125**: 557–571.

J Pharmacol Sci 97, 525 – 532 (2005)

Journal of Pharmacological Sciences

Full Paper

Altered Brain Penetration of Diclofenac and Mefenamic Acid, but Not Acetaminophen, in Shiga-Like Toxin II-Treated Mice

Masaya Fukuda[1], Kiyoyuki Kitaichi[1,*], Fumie Abe[1], Yohei Fujimoto[1], Kenji Takagi[1], Kenzo Takagi[1], Tsuneo Morishima[2], and Takaaki Hasegawa[3]

[1]*Department of Medical Technology, Nagoya University School of Health Sciences, 1-1-20 Daikominami, Higashi-ku, Nagoya 461-8673, Japan*
[2]*Department of Pediatrics, Okayama University School of Medicine, 2-5-1 Shikada-cho, Okayama 700-8558, Japan*
[3]*Department of Hospital Pharmacy and Pharmacokinetics, Aichi Medical University School of Medicine, Nagakute-cho, Aichi-gun, Aichi 480-1195, Japan*

Received October 13, 2004; Accepted February 28, 2005

Abstract. It is well accepted that bacterial and virus infections elevate the levels of cytokines in serum and cerebrospinal fluids. Such high levels of cytokines might alter the integrity of the blood-brain barrier (BBB) and/or blood-cerebrospinal fluid barrier (BCSFB), subsequently affecting brain penetration of drugs. However, few reports have addressed this issue. Thus, we investigated brain penetration of cyclooxygenase (COX) inhibitors, commonly used as antipyretics, in mice treated with Shiga-like toxin II (SLT-II) derived from *E. coli* O157:H7, which significantly elevates cytokine levels. As antipyretics, we used diclofenac, mefenamic acid, and acetaminophen. We found that SLT-II significantly increased the brain-to-plasma concentration ratio (K*p*) of diclofenac and mefenamic acid, but not of acetaminophen. Moreover, the K*p* of diclofenac and mefenamic acid was increased by probenecid, an anionic compound. These results suggest that efflux anion transporters might be involved in the transport of diclofenac and mefenamic acid. Western blot analysis revealed that SLT-II decreased the expression of organic anion transporter-3, an efflux transporter located on the BBB and/or BCSFB. Taken together, these results suggest that SLT-II and/or SLT-II-stimulated cytokines might change brain penetration of drugs and could possibly increase the risk of their side-effects by altering the expression of transporters.

Keywords: blood-brain barrier, Shiga-like toxin II, organic anion transporter, cyclooxygenase inhibitor

Introduction

Cyclooxygenase (COX) inhibitors are widely used as antipyretic drugs in patients with virus or bacteria infection with high fevers. The treatment with COX inhibitors is generally effective. However, when COX inhibitors are used in children, there may be central nervous system (CNS) complications such as Reye's syndrome (1). Moreover, the influenza-associated encephalopathy in the Asian population is reported to be worsened by COX inhibitors (2, 3), associated with higher levels of cytokines in serum (4, 5) and in cerebral spinal fluids (6).

It has been reported that cytokines might regulate the functions of transporters at the blood-brain barrier (BBB) and blood-brain cerebrospinal barrier (BCSFB) (7 – 9). Thus, it is likely that the influenza and influenza-like symptoms might stimulate the release of cytokines (4 – 6) that impair BBB function. Accordingly, BBB and/or BCSFB dysfunction might alter the penetration of COX inhibitors into the CNS, subsequently causing CNS damage. However, because of a lack of animal models, no reports have addressed this issue.

Recently, it has been demonstrated that Shiga-like toxin type II (SLT-II), a bacterial toxin from *E. coli* O157, stimulates significant release of cytokines in

*Corresponding author. FAX: +81-52-719-3009
E-mail: kitaichi@met.nagoya-u.ac.jp

rodents (10 – 12) and that SLT-II altered drug penetration into the brain (11). For example, the brain-to-plasma concentration ratio (K*p*) of fluorescein isothiocyanate labeled dextran (FD-4), a marker for the penetration through the tight junction of brain capillary endothelial cells at the BBB and BCSFB, was significantly increased (11). Moreover, it has been reported that the K*p* of doxorubicin was also increased in SLT-II-treated animals (11). One of the possible explanations for this alteration of the function of the BBB and/or BCSFB could be the significant release of inflammatory cytokines including tumor necrosis factor (TNF)-α, interleukin (IL)-6, IL-10, and nitric oxide (NO) by SLT-II (10 – 12), although the precise mechanism is not yet known.

Recently, various transporters have been found on the BBB and BCSFB that act as influx/efflux transporters (13, 14). It has been reported that the ability of several transporters to transport their substrates is competitively blocked by COX inhibitors (15, 16), suggesting that several COX inhibitors are transported at the BBB and/or BCSFB. For example, among organic anion transporters (OATs), OAT2 and OAT3 have been reported to be localized on the BBB and BCSFB (13, 15, 17 – 19). The OAT1- and OAT2-mediated transports in the transfected LLC-PK1 cells were blocked by various COX inhibitors (diclofenac, ketoprofen, indometacin, and others) (16, 20, 21). Moreover, organic anion transporting polypeptide (Oatp) 14 was localized on the BBB and BCSFB (22). The transport of prothyroid hormone in Oatp14-expressed HEK 293 cells was blocked by ketoprofen. Furthermore, two Oatps have been localized in the rat choroid plexus epithelium; Oatp2 is expressed at both the basolateral and apical membranes, while Oatp3 was identified at the apical membrane (13). The Oatp2-mediated transports were also blocked by ketoprofen and indometacin (23). Moreover, it has been reported that monocarboxylic acid transporters (MCTs) can transport several COX inhibitors that have a carboxyl residue (24). These results suggest the importance of transporters on the penetration of COX inhibitors into brain. However, the transporters responsible for COX inhibitors transport at the BBB and their functional and biochemical changes in response to infection including influenza are not well understood.

In the present study, we investigated brain penetration of COX inhibitors in a mouse model of infection associated with high levels of cytokines. We selected SLT-II-treated mice as the BBB failure model during the infection. Among COX inhibitors, diclofenac, mefenamic acid, and acetaminophen were studied.

Materials and Methods

Materials

Diclofenac, mefenamic acid, and probenecid were purchased from Sigma (St. Louis, MO, USA). Acetaminophen was purchased from Wako (Osaka). All other reagents were commercially available and were of analytical grade. All chemicals were dissolved in physiological saline before use.

Preparation of SLT-II

A clinically isolated *E. coli* O157:H7 strain NGY12 was used for the production of SLT-II as reported previously (12). This strain does not produce SLT-I. The absence of SLT-I gene was confirmed by PCR with specific primers. The strain was grown in 500 ml Luria broth (LB) by constant shaking for 12 h at 37°C. The culture supernatant was obtained by centrifugation and the protein fraction was precipitated with 60% saturated ammonium sulfate at 4°C. The precipitate was collected by centrifugation, dissolved in 2 ml of phosphate-buffered saline (PBS) (pH 7.2) and dialyzed overnight against PBS at 4°C. After the dialysis, the dialysate (approximately 2.5 ml) was used as the crude SLT-II preparation. The concentration of SLT-II in the crude preparation was determined to be 20 μg/ml by using a reverse passive latex agglutination kit (Vtec-Rpla; Denka Seiken, Tokyo).

Animals

Male ddY mice (Japan SLC, Hamamatsu), weighing 25 – 30 g, were used in this study. The mice were housed under controlled environmental conditions (about 25°C) with commercial food and water freely available. All animal experiments were carried out in accordance with the guidelines of Nagoya University School of Medicine for the care and use of laboratory animals.

Establishment of SLT-II-treated mice

SLT-II-treated mice were established by injecting SLT-II (0.3 μg/animal) into the tail vein of mice 24 h before starting the experiments (11). Control mice were injected with saline instead of SLT-II.

Protein binding experiments

To measure the protein binding of each drug in the control and SLT-II-treated mice, the protein binding experiment was done by using seamless cellulose tubing (Viskase Sales Corp., Willowbrook, IL, USA). Plasma samples were obtained from control mice and mice treated 24 h earlier with SLT-II (0.3 μg/animal). Before doing the experiment, the seamless cellulose tubing was boiled for 1 h. Plasma sample was put into one side of a

dialysis cell divided by the seamless cellulose tubing, and PBS containing each drug (10 μg/ml) was put into the other side. Then, they were incubated for 6 h at 37°C. The total (plasma solution) and unbound (PBS solution) concentrations of each drug were measured by high-performance liquid chromatography (HPLC).

In vivo experiments

Mice were anesthetized with pentobarbital (25 mg/kg) and cannulated with polyethylene tubes (PE 28; Natsume, Tokyo) in the right jugular vein for drug administration and blood collection. After surgical preparation, mice received a loading dose (LD) and a maintenance dose (MD) of COX inhibitors at a rate of 0.3 ml/h until the end of the study. The LD and the MD of each drug were as follows: diclofenac: LD = 1.70 mg/kg, MD = 1.88 mg·h^{-1}·kg^{-1}; mefenamic acid: LD = 15.35 mg/kg, MD = 12.32 mg·h^{-1}·kg^{-1}; acetaminophen: LD = 46.27 mg/kg, MD = 12.10 mg·h^{-1}·kg^{-1}. Based on the preliminary experiments to obtain plasma concentrations-time profiles of COX inhibitors after the bolus intravenous injection of diclofenac (10 mg/kg), mefenamic acid (10 mg/kg), and acetaminophen (100 mg/kg), the corresponding pharmacokinetic parameters were calculated and LD and MD were decided upon. Expected plasma concentrations of COX inhibitors were 15 μg/ml of diclofenac, 15 μg/ml of mefenamic acid, and 10 μg/ml of acetaminophen. After 2-h infusion, the mice were killed by exsanguinations, and blood and brain samples were collected.

To evaluate the function of anion transporter in the brain, a typical anion transporter inhibitor, probenecid, was administered to the mice. Probenecid was administered (100 mg/kg, i.p.) to control and SLT-II-treated mice 30 min before they were killed. The dose of probenecid was selected from the literature and is known to induce efflux transport of anionic compounds from the brain (25, 26). The control and SLT-II group without probenecid were administrated saline (0.1 ml/10 g, i.p.) instead of probenecid. The mice were killed by exsanguinations, and blood and brain samples were collected.

Blood samples were immediately centrifuged at 6,000 rpm for 10 min at 4°C to yield plasma. Brain samples were homogenized with a 4-fold volume of saline by an ice-cold glass homogenizer. All plasma and brain samples were stored at −80°C until analysis.

The Kp value of each drug is presented as the brain-to-plasma concentration ratio:

Kp_{total} = brain concentration / Css

$Kp_{unbound}$ = brain concentration / Css × unbound fraction

Extraction of COX inhibitors from plasma and brain tissue

For quantification of mefenamic acid and diclofenac, 50 μl of plasma samples or 200 μl of brain samples were vortexed for 10 min with 10 μl of internal standard (I.S.), 10 μl of HCl, and 1000 μl of hexane / isopropanol (99 : 1). Mefenamic acid (50 μg/ml) was used as I.S. for diclofenac measurement and diclofenac (50 μg/ml) for mefenamic acid measurement. After the centrifugation at 12,000 rpm for 5 min at 4°C, 900 μl of upper organic solvent layer was collected into test tubes and evaporated to dryness under a stream of nitrogen gas at 30°C. The dried residues were reconstituted with 120 μl of the mobile phase and injected into the HPLC instrument.

To extract acetaminophen from plasma and brain tissue, 50 μl of plasma samples or 200 μl of brain samples were vortexed for 10 min with 500 μl of methanol containing antipyrine (5 μg/ml) as an I.S. After the centrifugation at 12,000 rpm for 5 min at 4°C, 450 μl of the upper organic solvent layer was collected into test tubes and evaporated to dryness under a stream of nitrogen gas at 40°C. The residue was reconstituted with 120 μl of the mobile phase and injected into the HPLC instrument.

Analysis of COX inhibitors in plasma and brain samples by HPLC

After the extraction, plasma and brain concentrations of each drug were determined by HPLC.

The HPLC apparatus was an LC-10A$_{VP}$ system (Shimadzu, Kyoto) consisting of an LC-10A$_{VP}$ liquid pump, an SPD-10A$_{VP}$ ultraviolet detector, and an SIL-10A$_{VP}$ autoinjector. A Cosmosil 5C18-MS-II column (4.6 × 150 mm; Nacalai Tesque, Kyoto) was used with a column oven (OTC-10A$_{VP}$, Shimadzu) heated to 40°C. A voltage stabilizer (CV-1000; Denken Co., Ltd., Aomori) was also used.

In order to analyze diclofenac and mefenamic acid, 0.1 M phosphate buffer (pH 5.0) : acetonitrile = 60 : 40 (vol : vol) was used as the mobile phase at 1.2 ml/min flow rate, and the column eluate was monitored at a UV wavelength of 279 nm (27, 28).

To analyze for acetaminophen, 0.1 M phosphate buffer (pH 5.0) : methanol = 85 : 15 (vol : vol) was used as the mobile phase at 1.0 ml/min flow rate, and the column eluate was monitored at a UV wavelength of 245 nm (29).

Standard curves for measuring COX inhibitors in the plasma and brain tissue were linear for concentrations ranging from 0.15 to 20 μg/ml, with a correlation coefficient of 0.999. The intra- and inter-assay coefficients of variation for the HPLC assay were less than 6%

at concentrations of 0.15 to 20 μg/ml. The detection limit of COX inhibitors was 0.05 μg/ml.

Western blot analysis

Brain obtained from control mice (saline) and mice treated 24 h after SLT-II (0.3 μg/animal, i.v.) was kept at −80°C until analysis. Each brain was homogenized with a 5-fold volume of homogenate buffer (0.1 M Tris-HCl buffer (pH 8.0) containing 1 mM phenylmethylsulfonyl fluoride (PMSF), 1 mM dithiothreitol (DTT), aprotinin, leupeptin, pepstatin) in a glass homogenizer at 4°C. Then the homogenate was re-homogenized with a loose dounce homogenizer. After obtaining the homogenate supernatant by centrifugation at 8,500 rpm for 15 min at 4°C, the supernatant was transferred to an ultracentrifuge tube and centrifuged at 40,000 rpm for 30 min at 4°C. Subsequently, the supernatant was removed and the pellet was dissolved in homogenate buffer containing 1% of NP-40.

The protein concentration in the solution was measured using the Bio-Rad Protein Assay (Bio-Rad, Richmond, CA, USA) with bovine serum albumin (Sigma) as a standard. The protein (25 μg per lane) was subjected to electrophoresis on a 10% sodium dodecylsulfate (SDS)-polyacrylamide gel. The separated proteins were electrotransferred onto a nitrocellulose membrane, and the membrane was blocked with PBS containing 0.1% Tween 20 (PBS-T) and 5% nonfat dry milk for 1 h at room temperature. After washing three times with PBS-T for 5 min, the membrane was incubated with anti-OAT3 antibody (Transgenic, Kumamoto) for 1 h at room temperature. After washing three times, the membrane was allowed to bind a horseradish peroxidase-labeled anti-rabbit IgG antibody (Amersham Biosciences UK Ltd., Little Chalfont, UK) diluted 1 : 1000 in PBS-T for 1 h at room temperature. After washing three times, the bands were detected using ECL plus (Amersham Biosciences UK Ltd.). To quantify the relative levels of OAT3 in membranes, intensity of the stained bands was measured by the NIH image program (National Institutes of Health, Bethesda, MD, USA).

The statistical analysis

Results are expressed as the mean ± S.E.M. Data were analyzed by one-way analysis of variance (ANOVA) and post-hoc comparison was carried out with the Scheffe's post-hoc test. All statistics reported in these experiments were generated using StatView (version 4.5; Abacus Concepts, Berkeley, CA, USA) and *P*-values less than 0.05 were considered statistically significant.

Results

Plasma, brain concentrations and Kp of each COX inhibitor in control mice

COX inhibitors were continually infused until plasma steady-state concentrations were reached, at which point plasma and brain concentrations of COX inhibitors were measured. The ratio of brain concentration to total plasma concentration of COX inhibitors (Kp_{total}) varied between COX inhibitors. The rank of order of Kp_{total} was observed to be acetaminophen (0.773 ± 0.074) > diclofenac (0.048 ± 0.003) > mefenamic acid (0.039 ± 0.006) when calculated using total plasma concentrations (Table 1). Since drug binding to plasma protein could affect drug distribution and elimination kinetics, the protein binding of the three COX inhibitors was also measured. The unbound fraction of diclofenac, mefenamic acid, and acetaminophen was $0.068 \pm 0.008\%$, $19.58 \pm 1.48\%$, and $89.55 \pm 2.28\%$, respectively (Table 1). Based on these results, the ratio of brain concentration to unbound plasma concentration of COX inhibitors ($Kp_{unbound}$) was calculated. The rank of order of $Kp_{unbound}$ was diclofenac (71.057 ± 3.786) ≫ acetaminophen (0.863 ± 0.083) > mefenamic acid (0.198 ± 0.029) (Table 1).

Effects of SLT-II on protein binding and Kp of COX inhibitors

To investigate the effect of SLT-II on the penetration of COX inhibitors into brain, Kp of each drug was studied in mice pretreated with SLT-II. In SLT-II-treated mice, for each COX inhibitor tested, protein binding was not altered. The unbound fraction of diclofenac, mefenamic acid, and acetaminophen was $0.065 \pm 0.004\%$, $16.71 \pm 0.08\%$, and $85.55 \pm 1.09\%$, respectively (Table 2). Kp_{total} of acetaminophen was not significantly different between control and SLT-II-treated mice (Fig. 1, Table 2). However, Kp_{total} of diclofenac and mefenamic acid was significantly increased in SLT-II-treated mice (Fig. 1, Table 2). No significant differences in the plasma concentrations of each drug were observed between the control and SLT-II-treated mice (Table 2).

Effects of probenecid on Kp in control and SLT-II-treated mice

In order to investigate the involvement of the anion transport system in brain penetration of COX inhibitors, we coupled administration of COX inhibitors with the typical anionic compound probenecid. In control mice, probenecid significantly increased the Kp_{total} of both diclofenac and mefenamic acid (Fig. 2). However, in SLT-II-treated mice, probenecid did not affect the Kp_{total}

Table 1. Plasma, brain concentration, and protein binding (unbound fraction: fu) of each COX inhibitor in control mice

Drugs	Plasma (μg/ml)	Brain (μg/ml)	fu (%)	Kp (total)	Kp (unbound)
Diclofenac	15.11 ± 1.72	0.72 ± 0.06	0.068 ± 0.008	0.048 ± 0.003	71.06 ± 3.79
Mefenamic acid	18.05 ± 2.96	0.59 ± 0.06	19.58 ± 1.48	0.039 ± 0.006	0.198 ± 0.029
Acetaminophen	7.83 ± 1.23	5.79 ± 0.44	89.55 ± 2.28	0.773 ± 0.074	0.863 ± 0.083

Data represent the mean ± S.E.M. of 4 to 5 animals.

Table 2. Plasma, brain concentration, and protein binding (unbound fraction: fu) of each COX inhibitor in SLT-II-treated mice

Drugs	Plasma (μg/ml)	Brain (μg/ml)	fu (%)	Kp (total)	Kp (unbound)
Diclofenac	12.08 ± 2.14	0.84 ± 0.13	0.065 ± 0.004	0.072 ± 0.007[a]	110.38 ± 10.02[a]
Mefenamic acid	16.34 ± 2.00	1.78 ± 0.27[b]	16.71 ± 0.08	0.115 ± 0.015[b]	0.690 ± 0.091[b]
Acetaminophen	7.64 ± 1.13	5.58 ± 0.95	85.55 ± 1.09	0.725 ± 0.035	0.848 ± 0.041

Mice were treated with SLT-II (0.3 μg/animal) into the tail vein 24 h before drug administration. Data represent the mean ± S.E.M. of 4 to 5 animals. [a]P<0.05, [b]P<0.01 *vs* control group (Scheffe's post-hoc test).

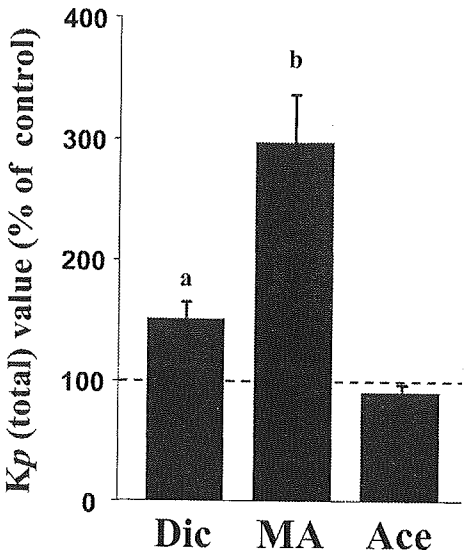

Fig. 1. Kp of Dic, MA, and Ace in SLT-II-treated mice. SLT-II was injected (0.3 μg/animal, i.v.) into the tail vein of mice 24 h before starting the experiments. Dic, MA, or Ace was continuously infused in SLT-II-treated mice. Two hours after the infusion of COX inhibitors, mice were killed to obtain Kp. Each column represents the ratio of the control mice and is presented as the mean ± S.E.M. (n = 4 – 5). [a]P<0.05 *vs* control. [b]P<0.01 *vs* control.

of both diclofenac and mefenamic acid (Fig. 2).

Expression of OAT3 in SLT-II-treated mice

Western blotting analysis revealed that the expression of organic anion transporter 3 (OAT3) in the brain was significantly decreased to 57 ± 5% of the control after 24 h of SLT-II treatment (Fig. 3).

Discussion

It is generally accepted that influenza virus infections stimulate the significant release of cytokines (4, 5), subsequently causing an infection-related syndrome including fever, diarrhea, and other symptoms. There are many reports indicating that cytokines affect the properties of the BBB and BCSFB by altering the function of the tight junction and drug/nutrition transporters (8, 10 – 12). However, the impact of the infection on brain penetration of antipyretic COX inhibitors remains unclear. Thus, we investigated brain penetration profiles of three COX inhibitors, diclofenac, mefenamic acid, and acetaminophen, that are popularly used as antipyretics, in the presence of SLT-II, a bacterial toxin, that stimulates cytokine release and alters the function of transporters as well as tight junctions in the brain (10 – 12).

Initially, we compared the brain penetration of each COX inhibitor using the ratio of brain concentration to unbound plasma concentration ($Kp_{unbound}$). Our results indicated that $Kp_{unbound}$ differed between COX inhibitors, with the rank of order of $Kp_{unbound}$ being diclofenac ≫ acetaminophen > mefenamic acid. These data suggest that diclofenac might potentially penetrate into brain more so than other COX inhibitors used in this study. Secondly, the effect of SLT-II on brain penetration of COX inhibitors was investigated. We found that Kp values of diclofenac and mefenamic acid were significantly increased, but not that of acetaminophen. In addition, SLT-II did not affect protein binding of all COX inhibitors. Taken together, these data show that SLT-II changed brain penetration of diclofenac and mefenamic acid, but not acetaminophen. Moreover, it

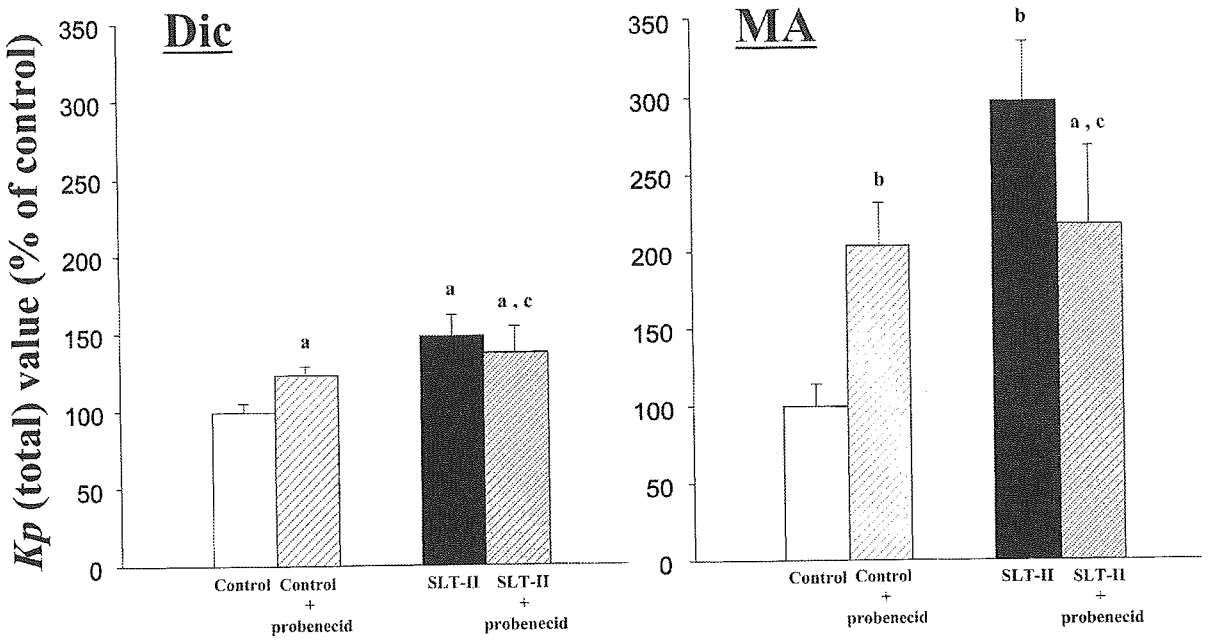

Fig. 2. Effect of probenecid on K*p* of Dic and MA in control and SLT-II-treated mice. SLT-II was injected (0.3 μg/animal, i.v.) into the tail vein of mice 24 h before starting the experiments. Dic or MA was continuously infused in control mice and SLT-II-treated mice. Two hours after the infusion of COX inhibitors, mice were killed to obtain K*p*. Probenecid was administered (100 mg/kg, i.p.) 30 min before they were killed. Each column represents the mean ± S.E.M. $^{a}P<0.05$ *vs* control. $^{b}P<0.01$ *vs* control. $^{c}P>0.05$ *vs* SLT-II.

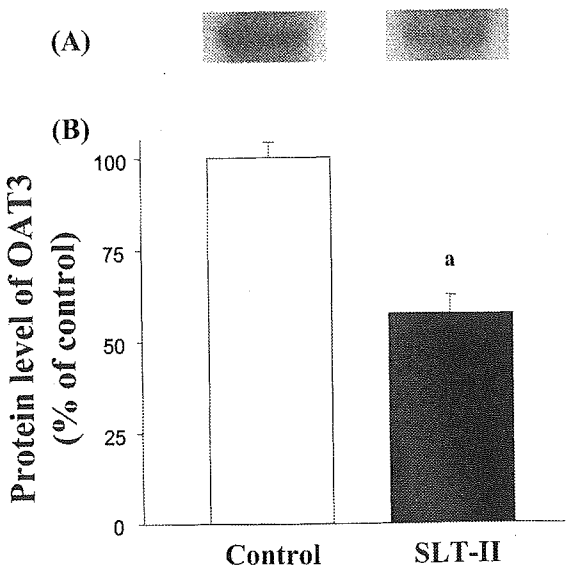

Fig. 3. Effect of SLT-II on the protein level of OAT3 in brain (A) and ratio of relative staining intensity for OAT3 in control and SLT-II-treated mice (B). Brain samples were obtained from control mice (saline) and mice treated 24 h after SLT-II (0.3 μg/animal, i.v.). The band was detected at approximately 50 kDa. Each column represents the mean ± S.E.M. $^{a}P<0.01$ *vs* control.

has been suggested that among the COX inhibitors investigated, it would be easier to control acetaminophen dosage because less consideration for potential CNS side-effects is needed.

In a previous study, we demonstrated that the same dosing regimen of SLT-II increased the brain to plasma ratio of fluorescein isothiocyanate labeled dextran with average molecular weight 4.4 kDa (FD-4), to approximately 150% of the control (11). In the present experiment, brain penetration of diclofenac and mefenamic acid increased to 148 ± 13% and 297 ± 39% of the control. Thus, SLT-II might alter an active transport system for COX inhibitors, in addition to changing brain capillary integrity. We also previously demonstrated that SLT-II increased the brain to plasma ratio of doxorubicin (11). Considering the fact that doxorubicin is a typical substrate for one of the efflux transporters, P-glycoprotein, it would be expected that SLT-II decreased P-glycoprotein expression, subsequently decreasing the efflux of doxorubicin into the blood circulation. However, unexpectedly, SLT-II did not decrease P-glycoprotein expression, but rather increased it (11). Thus, these results suggest that SLT-II might modify the expression of other transporters sensitive to doxorubicin (11).

In the present study, SLT-II increased brain penetration of diclofenac and mefenamic acid, but not acetaminophen. Strictly speaking, diclofenac and mefenamic acid, but not acetaminophen, having a carboxyl group is negatively charged under the physiological condition. Thus, it is likely that SLT-II might alter the expression of anion transporters rather than P-